CircPDK1 promotes RCC cell migration and invasion through the *miR-377-3p/NOTCH1* axis

Zhenlin Huang
the First Affiliated Hospital of Zhengzhou University
Yinghui Ding
the First Affiliated Hospital of Zhengzhou University
Lu Zhang
Renmin Hospital of Wuhan University
Siyuan He
the First Affiliated Hospital of Zhengzhou University
Zhangkui Jia
the First Affiliated Hospital of Zhengzhou University
Chaohui Gu
the First Affiliated Hospital of Zhengzhou University
Tao Wang
the First Affiliated Hospital of Zhengzhou University
Hao Li
the First Affiliated Hospital of Zhengzhou University
Xiang Li
the First Affiliated Hospital of Zhengzhou University
Zhibo Jin
the First Affiliated Hospital of Zhengzhou University
Yafei Ding
the First Affiliated Hospital of Zhengzhou University
Jinjian Yang (hzlinok@outlook.com)
the First Affiliated Hospital of Zhengzhou University https://orcid.org/0000-0002-3453-2692

Research

Keywords: CircPDK1, miR-377-3p, NOTCH1, RCC, Metastasis

Posted Date: March 4th, 2020

DOI: https://doi.org/10.21203/rs.3.rs-15935/v1

Abstract

Circular RNAs (circRNAs) are novel clusters of endogenous noncoding RNAs (ncRNAs) that are widely expressed in various tissue types. Recent studies have indicated that circRNAs involved in multiple tumorigenesis processes, and the potential significance of circRNAs remains to be explored. However, the roles roles and underlying mechanisms of circRNAs in clear cell renal cell carcinoma (RCC) remain unclear. We found that *CircPDK1* is highly expressed in RCC by circRNA-seq assay. Moreover, the functional enrichment experiments showed that *CircPDK1* is significantly associated with RCC metastasis. Eighty pairs of clinical samples were analyzed, and the results showed a correlation between *CircPDK1* and lymph node and distant organ metastases in RCC. RNA-sequencing following knockdown of *CircPDK1* revealed significant changes in the expression of many molecules in the metastasis-associated pathway. After bioinformatics prediction, we verified the relationships between *CircPDK1* and *miR-377-3p* and between *miR-377-3p* and *NOTCH1* by a luciferase reporter assay. Furthermore, the effect of *CircPDK1* on RCC metastasis can be functionally influenced by *miR-377-3p* and *NOTCH1*. Altogether, our study shows that the *CircPDK1* - *miR-377-3p* - NOTCH1 axis plays an important role in RCC metastasis, suggests *CircPDK1* might serve as a potential therapeutic target for RCC treatment.

Background

Renal carcinoma (RCC) is currently the seventh most common type of cancer in the world and is accompanied by more than 140,000 related deaths worldwide each year [1, 2]; among these deaths, clear cell renal carcinoma (ccRCC) accounts for more than 90% [3]. With the improvement of the examination and treatment methods, the 5-year survival rate of RCC had been greatly improved to exceed 70%. However, once tumor metastasis has occurred in the lungs, bones, brain, liver or other organs, its 5-year survival rate drops dramatically; therefore, metastatic RCC is considered one of the most malignant types of tumors [4, 5]. At the same time, the proportion of adolescent RCC metastasis was significantly higher than the proportion in the general population [5]. Previous treatments for distant metastases included immunotherapy with interleukin-2 and interferon-α, but clinical studies showed that only 13% of patients experienced complete or partial remission [6]. Although the new therapeutic methods mainly affect specific targets in biological pathways, such as the VEGF/PDGFR/mTOR pathway, providing a new therapeutic method, its side effects and limited sustained response rates remain an urgent problem [6]. All of this suggested that the metastatic RCC faces enormous challenges. Therefore, the constant search for the mechanism and treatment of metastatic RCC was one of the most important issues in RCC treatment.

Circular RNAs (circRNAs) were recently discovered as a class of widely expressed noncoding RNA [7] and have been indicated to be involved in gastrointestinal tumors, oral squamous cell carcinoma, malignant melanoma, nasopharyngeal carcinoma, bone tumor, myocardial fibrosis, bone differentiation and other many tumor types and biological processes [8–13]. Because of the ring-like structure with no 5' to 3' polarity, circRNAs usually have a relatively stable structure, but their function also showed differences with other noncoding RNAs [14]. A growing number of studies have shown that cytoplasmic circRNAs act

primarily through the adsorption of microRNA (miRNA) by the sponge effect, and the adsorption of miRNA by circRNA limits its ability to bind to the 3'UTR region of the messenger RNA (mRNA) [15]. MiRNAs are single stranded ncRNAs of approximately 19–25 nucleotides in length and involved in post transcriptional regulation by binding the 3'UTR region of the mRNAs [16].

There are few studies on circRNA in the kidneys, especially on RCC [17–19]. In our study, we used five pairs of RCC and adjacent tissues to perform circular RNA sequencing and identified many differentially expressed CircRNAs, such as circ12132, circRNA2976, circRNA1526, and circRNA2326. Further, we analyzed the enrichment of circRNAs in RCC through functional and pathway analysis to identify the potentially important mechanism of circRNA in the development of RCC. We identified a novel circRNA CircPDK1, which was significantly upregulated in RCC by circular RNA sequencing and qRT-PCR and explored its biological function and mechanism.

Materials And Methods

1. Patients and renal tissues

A total of 102 pairs fresh-frozen RCC tissues and paired paratumor tissues were collected from patients who underwent renal tumor resection surgery in the First Affiliated Hospital of Zhengzhou University from January 2014 to December 2017. All tumor tissues passed the neuropathological criteria of having > 80% tumor nuclei and < 50% necrosis, and the final histological diagnosis was made on formalin-fixed, paraffin-embedded tissue samples due to the result of hematoxylin and eosin (H&E) staining and immunochemistry. Among these, we used a cohort of 5 patients (RCC and paratumor tissues) to screen the differential expression of circRNAs. 30 pairs of tissues were used to undergo qRT-PCR to verify the expression of CircPDK1. In addition, the CircPDK1 level in all 80 patients was analyzed for its functional relationship with clinical features. Our study was approved by the Ethics Committee of the First Affiliated Hospital of Zhengzhou University.

2. Cell culture and cell lines

All the RCC cell lines 786-0, 769-P, ACHN and normal kidney cell lines HK-2 and 293T were purchased from the Culture Collection of Chinese Academy of Sciences (Shanghai, China). 786-0 and 769-P cells were maintained in RPMI-1640 medium with 10% fetal bovine serum (Gibco, US) and 1% penicillin/streptomycin (Sigma, USA). ACHN cells were maintained in MEM with 10% fetal bovine serum (Gibco, USA) and 1% penicillin/streptomycin (Sigma, USA). HK-2 cells were maintained in keratinocyte medium (ScienCell, USA) with 1% keratinocyte growth supplement (ScienCell, USA) and 1% penicillin/streptomycin (ScienCell, USA). 293T cells were maintained in DMEM with 10% fetal bovine serum (Gibco, USA) and 1% penicillin/streptomycin (Sigma, USA). All cells were cultured in the incubator with 5% carbon dioxide at 37 °C.

3. CircRNA-seq

Total RNA was extracted using TRIzol Reagent (Invitrogen, USA) following the manufacturer's procedure. The total RNA quantity and purity were analyzed by a Bioanalyzer 2100 and an RNA 6000 Nano LabChip Kit (Agilent, USA) with an RIN number > 7.0. Approximately 10 μg of total RNA from each sample was subjected to the Epicenter Ribo-Zero Gold Kit (Illumina, San Diego, USA) to remove ribosomal RNA prior to the construction of the RNA-seq libraries. Then, the rRNA-depeted RNA are fragmented into small pieces using divalent cations under elevated temperature. The cleaved RNA fragments were reverse-transcribed to create the final cDNA library following the protocol for the TruSeq Stranded Total RNA HT Sample Prep Kit (Illumina, San Diego, USA), and the average insert size for the paired-end libraries was 300 bp (± 50 bp). Then, we performed paired-end sequencing on an Illumina X Ten at LC Bio, China, in accordance with the vendor's recommended protocol. Raw data were normalized by the quantile algorithm and the limma packages in R, and we used Poisson distribution to determine the read number for specificity to clarify the specific circRNAs in each cancerous aged-matched normal tissue.

4. The analysis of CircRNA-seq data

Firstly, Cutadapt(v1.9)was used to remove the reads that contained adaptor contamination, low quality bases and undetermined bases. Then sequence quality was verified using FastQC (http://www.bioinformatics.babraham.ac.uk/projects/fastqc/). We used HISAT2 to map reads to the genome of (species). Remaining reads (unmapped reads) were still mapped to genome using tophat-fusion (v2.0.10). CIRCExplorer was used to denovo assemble the mapped reads to circRNAs at first, then, back splicing reads were identified in unmapped reads by tophat-fusion and CIRCExplorer. All samples were generated unique circRNAs. The differentially expressed circRNAs were selected with log2 (fold change) > 1 or log2 (fold change) <-1 and with statistical significance (p value < 0.05) by R package–edgeR.

5. Quantitative real-time PCR analysis

Total RNA was extracted from tissues with TRIzol Reagent (TaKaRa, Japan) according to the manufacturer’s protocol. The isolate RNA was transcribed into cDNA using a reverse transcription kit (TaKaRa, Japan). qRT-PCR was performed to quantify the RNA expression using a standard protocol from SYBR Green PCR Kit (Roche, USA) on the StepOne plus qRT-PCR System (ABI, USA). All PCR primers were purchased from RiboBio Co., Ltd. (Guangzhou, China) (primer list in Table 1). PCR was conducted at 95 °C for 30 s followed by 40 cycles of 95 °C for 5 s and 60 °C for 30 s. Each sample was analyzed in triplicate, and the relative expression was calculated using the $2^{-\Delta\Delta Ct}$ method relative to that of GAPDH.

6. Fluorescence in situ hybridization (FISH)

To locate the CircPDK1 distribution in RCC cells, we designed the FISH assay to detect the details. A FISH-specific target CircPDK1 RNA probe (RiboBio Co., Ltd., China) was labeled by CY3, and we chose U6 and 18S as references for nuclear localization and cytoplasmic localization, respectively. The cell slides were placed in the bottom of a 24-well plate and incubated the appropriate amount of cells (6×10^4 cells/well, the cell fusion degree was 60%-70% before the experiment), then the cells were washed with 1x PBS and

fixed with 4% paraformaldehyde for 10 min at room temperature. After washing the cells with 1 x PBS, 200 μL of prehybridization solution (mixed with blocking solution and prehybridization buffer at a ratio of 1:99) and 2.5 μL of 20 μM FISH Probe Mix or internal reference FISH Probe Mix was added. After discarding the prehybridization solution, an appropriate amount of probe-containing hybridization solution containing the probe was added, and the samples were hybridized overnight at 37 °C protected from light. The slides were washed with washing solution and 1 x PBS the next day and then stained with DAPI staining solution for 10 min before mounting. Images were obtained using a laser scanning confocal microscope (Leica, Germany) at 400x magnification.

7. CircPDK1 overexpression or knockdown cell line construction and vector transfection

The pHBLV-CircPDK1-OE plasmid was synthesized by Hanbio Co., LTD. (Shanghai, China), and the sh-CircPDK1, miR-377-3p mimics and miR-377-3p inhibitor plasmids were synthesized by RiboBio Co., Ltd. (Guangzhou, China). pHBLV-CircPDK1-OE or sh-CircPDK1 lenti virus was cotransfected into the 293T cell line with pSPAX2 and pMD2.G by using Lipofectamine 3000 (Invitrogen, USA); the virus was collected approximately 48 h later. Stable knockdown cell lines were constructed by transfection with lentivirus and polybrene (Invitrogen, USA) and were selected with medium containing 2% puromycin. The transfection efficiency was tested by qRT-PCR. For transient transfection, the cell lines were seeded in 6-well plates at a concentration of 2.5×10^5 cells/well and transfected with miR-377-3p mimics, miR-377-3p inhibitors or pDONR-NOTCH1 (Addgene, USA) as indicated in the manuscript. The medium was replaced after 24 h and incubated for up to 48 h. Each experiment was repeated three times independently.

8. MTT (3-(4,5-dimethylthiazol-2-yl)-2,5-diphenyl tetrazolium bromide) assay

The MTT kit was purchased from RiboBio Co., Ltd. (Guangzhou, China). After the cells were seeded and grown in 96-well plates for a certain time with 200 μl medium, 10 μl of MTT reagent was added to each well at the appropriate concentration. The absorbance at 0, 24, 48, 72, 96 h in 469 mm was measured by a microplate reader.

9. Cell migration and invasion experiment

BD Matrigel and serum-free medium were diluted and mixed at a ratio of 1:8; 80 μl of the mix were pipetted into the upper chamber of the transwell and placed in the incubator for at least 2 h for the Matrigel invasion assay. RCC cell suspensions of 2.5×10^5 cells cells/ml were seeded into the transwell plate (for migration assay without BD Matrigel in the plate), and the chamber was placed in the plate. A total of 500 μl of complete medium containing 20% FBS was added to the transwell plate. Plate was cultured in a CO_2 (content 5%) incubator at 37 °C for 24 h, then the cells were stained with crystal violet for 10 min. Images were obtained using a microscope (Leica, Germany)

10. Wound-healing assay

RCC cells were seeded into 6-well plates at a density of 80%-90% and then scratched perpendicularly to the bottom of the plate. After washing with PBS and adding serum-free medium, the plates were cultured in a 37 °C incubator containing 5% CO_2, and the pictures were taken at the scheduled time.

11. Flow cytometry assay for apoptosis and cell cycle identification

The Annexin V-FITC PI Apoptosis Detection Kit and Cell Cycle Detection Kit were purchased from Solarbio (Beijing, China). 786-0 and ACHN cell lines were treated with plasmid for more than 48 h and stained with Annexin V-FITC/ PI for cell apoptosis; all the procedures followed the manufacturer's instructions. Imagines obtained by using flow cytometry (Leica, Germany) and analysis with ModFit LT software.

12. In vivo mouse experiments

Six-week-old male BALB/c nude mice were purchased from Charles River Laboratories (Beijing, China). CircPDK1-OE or the control vector was stably transfected into 786-0 cells that were harvested until the total cell number was approximately $1*10^6$. The mice were divided into two groups, and the cells were injected in the tail vein of each mouse in the two groups (each group had 10 mice). One month later, the mice were sacrificed, their lung tissues were removed and fixed with paraformaldehyde, and the number of metastatic nodules in the lung tissue was counted. All animal studies were approved by the Institutional Animal Care and Use Committee of the First Affiliated Hospital of Zhengzhou University.

13. RNA-seq

RNA was extracted as previously described using the circRNA extraction procedure from sh-CircPDK1 AND sh-control 786-0 and ACHN cell lines. RNA-seq was performed at Novogene Co., Ltd. (Beijing, China). Raw data were normalized by the Quantile algorithm, limma packages in R. The differentially expressed mRNAs were selected with log2 (fold change) > 1 or log2 (fold change) <-1 and with statistical significance (p value < 0.05) by the R package Ballgown.

14. Western blotting

The cells were lysed using RIPA, and the supernatant was retrieved after centrifugation. Then, the protein concentration was measured using a DC protein detection kit. After the protein was detached from the fillister and transferred to the PVDF membrane, it was incubated with a primary antibody overnight following incubation with 5% (5 g/100 mL) nonfat dry milk (Bio-Rad, USA) blocking for one hour. One hour after incubation in the HRP-conjugated secondary antibody, images were taken on the machine with ECL Luminescent liquid. The results were analyzed by Immobilon™ Western Chemiluminescent HRP Substrate (Millipore). β-Tubulin was used as a control. The primary antibodies used were anti-NOTCH1 (#3608, Cell Signaling Technology), anti- β-Tubulin (#2128, Cell Signaling Technology).

15. Luciferase reporter assays

The potential interactions between CircPDK1 and miR-337-3P or miR-337-3P with NOTCH1 were predicted by circRNA-seq data. By using pSI-Check2 as a template, we constructed hsa-NOTCH1-3'UTR-wt, hsa-NOTCH1-3'UTR-mu, hsa-CircPDK1-wt and has-CircPDK1-mu plasmids and transfected them into a 293T cell line. Then, a Promega Dual-Luciferase System (Hanbio Co., LTD., China) was used to detect the Renilla luciferase score in different groups, which can reflect the interaction between miR-377-3p with CircPDK1 and with NOTCH1.

16. Statistical analysis

All data are indicated as the means ± standard error of the mean (SEM) processed by GraphPad Prism 8.0 (La Jolla, USA) and IBM SPSS Statistics 20.0 (IBM, USA). Student's t-test, one-way ANOVA, Cox regression, and LSD-t-test, Pearson chi-square test, log-rank test, and linear regression analyses were used to evaluate the group differences. $P < 0.05$ was considered to have a significant change.

Results

CircRNA expression profiles analysis

To detect the circRNAs associated with RCC, we acquired five pairs of RCC tissues and paired paratumor tissues and performed circRNA-seq analysis. We detected 201821 circRNAs and 20809 of these exhibited differential expression between RCC and normal tissues (fold change > 2.0, $P < 0.05$); among these, 11220 circRNAs were upregulated and 9589 were downregulated in cancer tissues, and each differentially expressed circRNA displayed as a red dot in the volcano plot and separately as either a red dot or green dot in the scatter plot (Fig. 1A, B). The top 100 differentially expressed circRNAs are shown separately in the heat map (Fig. 1C). We used R package ggplot2 and local Perl scripts to analyze the statistical enrichment OD of the host genes of those differentially expressed protein-coding transcripts in the Gene Ontology (GO) terms and Kyoto Encyclopedia of Genes and Genomes (KEGG) pathway analysis (Fig. 1D, E). To confirm the expression of circRNAs and the RNA-seq data, qRT-PCR analysis was performed for 20 circRNAs randomly selected from the top 100 circRNAs of circRNA-seq results (Table 3). The results demonstrated that the qRT-PCR results were consistent with the RNA-seq results; this result confirmed that the circRNA-seq data are reliable. Among these, the magnitude of fold change was found in many circRNAs, such as circ12132, circRNA2976, circRNA1526, and circRNA2326 (Fig. 1F-I). Other circRNAs expression data showed in Table 3.

CircPDK1 is upregulated in RCC and is mainly located in the cytoplasm

In all circRNAs, we selected CircPDK1 (circ12132) for further study for its biggest fold change among the 20 selected CircRNAs, CircPDK1 is a circular RNA derived from the PDK1-201 transcript (Transcript ID: ENST00000282077.7) (sequences suppled in Supplemental 1), which contains 5 exons. CircPDK1 is formed by the middle part of the PDK1-201 transcript, which contains 5 exons (from the 2nd to 6th exon) (Fig. 2A, Supplemental 1). We designed primers to amplify the circular junctions, and qRT-PCR was implemented to further validate the expression of CircPDK1 in 30 pairs of RCC tissues and para tumor

tissues. Among which, CircPDK1 was significantly overexpressed in 24 pairs of tumor tissues (Fig. 1F, 2C), while its host gene PDK1 shows no different expression change in these 30 pairs tissues (Fig. 2D). The results are consistent with the results of circRNA-seq, which indicated that the expression of CircPDK1 is elevated in RCC tumor tissues. The same result can be further confirmed in the comparison of the renal tumor cell lines 786-0, 769-P, and ACHN with the normal kidney cell line HK-2, in which we found CircPDK1 overexpressed in the tumor cell lines (Fig. 2B). To investigate the localization of CircPDK1 in renal tumor cells, we constructed a specific probe for Cy3-labeled CircPDK1 and used 18S rRNA and U6 as nuclear and cytoplasmic reference genes, respectively. The results show that CircPDK1 is mainly enriched and localized in the cytoplasm (Fig. 2E). Plasmids were packaged and transfected into 786-0 and ACHN cells to construct stable knockdown or overexpressing cell lines, and we used qRT-PCR to test the transfection efficiency. The results showed that the expression level of CircPDK1 is significantly decreased or overexpressed in 786-0 and ACHN knockdown or overexpressing cell lines while the expression of PDK1 does not change significantly after overexpress or knock down circPDK1 (Fig. 2F-H). Correlation analysis of 60 pairs of clinical tissue samples showed that there was a significant correlation between CircPDK1 and lymph node metastasis and other organ metastasis of RCC, but there was no significant correlation with tumor growth and age, sex or other factors. These results showed that the high expression of CircPDK1 may play an important role in renal tumor metastasis (Table 2).

CircPDK1 promotes RCC cell invasion and metastasis

Because CircPDK1 is overexpressed in RCC, We further investigated the role of CircPDK1 in tumorigenesis and tumor metastasis in RCC by wound-healing, migration and Matrigel invasion assays. We found that the migration and invasion abilities of RCC cells were significantly inhibited after knockdown of CircPDK1 in both 786-0 and ACHN cell lines, although MTT proliferation assay and apoptosis assay showed that CircPDK1 did not greatly affect the proliferation and apoptosis of RCC cell lines after knock down of CircPDK1 (Fig. 3A-E). Futhermore, the effects of CircPDK1 on tumor metastasis in vivo was measured in a tumor xenograft model by injecting 786-0 cells overexpressing CircPDK1 or vector control via the tail vein. The results indicated that overexpressed CircPDK1 significantly promoted metastatic lung tumors compared with control group, suggesting that CircPDK1 is an independent factor that could promote RCC metastasis. (Fig. 3F). To explore the potential mechanism of CircPDK1, we used sh-CircPDK1 and sh-non-specific (NS) cells to perform RNA-sEq. The GO and KEGG analyses results showed that CircPDK1 strongly affected the process, such as extracellular interstitial component matrix interactions with the receptor and extracellular components, which are deeply involved in tumor metastasis. These results are also consistent with our clinical data and functional experimental results (Fig. 3G, H).

CircPDK1 directly binds to miR-377-3p in RCC

In tumor research, the use of circRNAs as miRNA “sponges” to regulate downstream target genes has been widely reported. We searched the RNA-seq data and bio-information tool to predict the potential miRNAs for CircPDK1. We found two complementary sequences between CircPDK1 and the miR-377-3p seed region (Fig. 4A). Then, we used a luciferase reporter assay to verify the potential influence between

them. As we predicted, the wild-type CircPDK1 luciferase activity was significantly curbed by miR-377-3p, while the mutated CircPDK1 luciferase activity had no influence on miR-377-3p, which means that miR-377-3p can directly bind to the CircPDK1 3'UTR region in these sites (Fig. 4B). Next, we explored the important role of miR-377-3p in RCC. qRT-PCR showed that miR-377-3p expression was decreased in RCC tumors or cell lines (Fig. 4C-D). Then, we treated 786-0 and ACHN cells with miR-377-3p-specific inhibitor or mimics, the RT-qPCR results showed that miR-377-3p was downregulated or upregulated compared with the NS groups, while it had no effect on CircPDK1 expression. These data suggest that CircPDK1 is upstream of miR-377-3p (Fig. 4E-G).

MiR-377-3p suppresses RCC cell invasion and metastasis by targeting NOTCH1

Based on the bio-information prediction results of our RNA-seq, we speculate that miR-377-3p may play a role by serving NOTCH1 as a substrate. To understand the mechanism, we transfected miR-377-3p mimics into 786-0 and ACHN cell lines. The qRT-PCR and Western blotting results showed that the RNA and protein expression levels of NOTCH1 were significantly decreased (Fig. 5A-C). In contrast, the RNA and protein expression levels of NOTCH1 were significantly increased after the miR-377-3p inhibitor was transfected into both 786-0 and ACHN cell lines (Fig. 5A-C). The clue that may further confirm its relationship in our hypothesis was that two direct potential target sites that may serve as the intermediates of miR-377-3p and NOTCH1 were identified. To further verify whether there is a direct effect between NOTCH1 and miR-377-3p, we designed clones of the NOTCH1 wild-type and mutant-type 3'UTR region (Fig. 5D). The dual-luciferase reporter assay showed that miR-377-3p mimics significantly downregulated the fluorescence of the NOTCH1 wild-type region and had no significant effect on the fluorescence of the NOTCH1 mutant-type region (Fig. 5E). To examine the role of miR-377-3p and NOTCH1 in in renal tumor cell lines, we performed a Matrigel invasion assay and a wound-healing assay after transfecting miRNA mimics or pDONR-Notch1 in 786-0 and ACHN cell lines, respectively. miR-377-3p mimic significantly decreased migration and invasion in RCC cells compared with control cells, and these effects were reversed by overexpression of NOTCH1 (Fig. 5F-G). Wound healing assay indicated that the miR-377-3p mimic led to slower closing of scratch wounds compared with the control group, while overexpression of NOTCH1 reversed these results (Fig. 5H-I). These results suggested that miR-377-3p involvement in RCC cells invasion and metastasis is mediated by the modulation of NOTCH1.

CircPDK1 promotes RCC cell invasion and metastasis by the sponge activity of miR-377-3p and the upregulation of NOTCH1

Since we had confirmed the relationship between miR-377-3p and NOTCH1, we were curious whether CircPDK1 could regulate the expression of NOTCH1 via miR377-3p. After knocking down CircPDK1, we used qRT-PCR and western blotting to detect the expression of NOTCH1 at the RNA and protein levels. The RT-PCR and western blot results showed that silencing CircPDK1 significantly downregulated NOTCH1 expression and miR377-3p inhibitor upregulated NOTCH1 expression (Fig. 6A-B). These results indicate that CircPDK1 and miR-377-3p are involved in the regulation of NOTCH1 in the same pathway. We found that CircPDK1 silencing significantly decreased the migration and invasion in RCC cells

compared with control cells, and these effects were reversed by inhibition of miR-377-3p or overexpression of NOTCH1 (Fig. 6D-E). A wound healing assay indicated that CircPDK1 silencing led to slower closing of scratch wounds compared with the control group, while inhibition of miR-377-3p or overexpression of NOTCH1 reversed these results (Fig. 6F- G).

These results confirmed that CircPDK1 could directly affect the invasion and migration of RCC cells by sponging miR377-3p.

Discussion

Although the treatment of RCC had made great progress with the advancement of diagnostic techniques and treatments, the significant characteristic of advanced RCC was often accompanied by the shedding of tumor thrombi and distant metastasis; once metastasis occurs, the 5-year survival rate drops significantly [6, 20, 21]. Therefore, preventing RCC metastasis has always been the focus of RCC treatment. In our study, we found a significant upregulation of CircPDK1 in RCCs. While in our chosen 30 paired RCC tissues, we didn't find its host gene PDK1 overexpression, which means CircPDK1 overexpression is not correlated with the PDK1 expression level. What's more, after overexpress or knockdown CircPDK1, PDK1 expression also not change significantly and those experiments confirm the CircPDK1 play its role independently. At the same time, clinical data analysis showed that although the expression of CircPDK1 was not correlated with the proliferation and apoptosis of RCC, it was obviously associated with lymph node metastasis and distant metastasis of renal tumors. To further explore the role of CircPDK1 in RCC, we performed a series of experiments after silencing CircPDK1 in RCC cell lines. The results of the wound-healing assay, migration assay, Matrigel invasion assay or mouse experiments in vivo were consistent with the clinical data. Furthermore, RNA-seq of sh-CircPDK1 indicated that CircPDK1 was mainly involved in the interaction between extracellular matrix components and their receptors. Mechanistically, CircPDK1 could function as a sponge by harboring miR377-3p and thereby abolishing the suppressive effect on the target gene NOTCH1 in RCC. Thus, our data suggest that CircPDK1 plays an important role in RCC metastasis.

CircRNAs are recently discovered as a special novel type of noncoding RNA whose function has not yet been elaborated and characterized by its highly conserved sequence and strong stability, which is considered by many researchers and doctors to be an important clinical diagnostic marker or therapeutic target, while the study of the role of circRNA in RCC is still unclear. The most common mechanism of action of circRNA includes 1) acting on miRNA through the sponge effect, thereby reducing the number of active miRNAs and inhibiting their effects on downstream target genes; 2) directly encoding the protein to function; and 3) directly functioning with its parental mRNA to prevent or promote its expression. In view of the obvious role of CircPDK1 in RCC metastasis, we hope to actively explore its mechanism of metastasis. Through our RNA-seq data and bioinformation prediction, we found that CircPDK1 potentially targets miR-377-3p. When we mutated their potential binding sites, their binding was significantly inhibited, which indicated a direct correlation between them.

miR-377-3p had been reported to be low-express in non-small-cell lung cancer (NSCLC), glioma cancer and breast cancer, in which miR-377-3p could inhibit the proliferation and metastasis of NSCLC and promote apoptosis of NSCLC by targeting E2F3 or HOXC6 [22–25], but its role in RCC still remains unclear. In our study, we first investigated miR-377-3p expression levels in renal tumor tissues and RCC cell lines. Similar to our expectation, miR-377-3p was significantly decreased in renal tumor tissue and renal tumor cell lines compared with the HK-2 cell line, which was regarded as normal renal cell. A wound-healing assay and Matrigel invasion assay showed that miR-377-3p can also inhibit the metastasis of RCC. Website prediction tools indicated that miR-377-3p possibly targets NOTCH1, which was one of the receptors involved in the Notch signaling pathway. NOTCH1 plays a role in preventing Notch signaling with N-terminal EGF-like repeats followed by LNR domains, which form a complex with ligands. The Notch signaling pathway is involved in processes such as cell proliferation, differentiation, and survival. The activation of NOTCH1 has been widely shown to be correlated with mammary tumorigenesis in animal models, and the upregulation of Notch receptors has been frequently observed in many cancer types. Furthermore, NOTCH1 has been shown to promote metastasis in many cancer types, including RCC, liver cancer, head and neck cancer, and gastric cancer [26–29]. It correlated with the formation of vasculogenic mimicry (VM) and the expression of epithelial-to-mesenchymal transition (EMT) biomarkers to be involved in the process of tumor metastasis [30, 31]. In our study, we found that miR-377-3p can interact with the 3’UTR of NOTCH1. Overexpression NOTCH1 reversed the decrease in cell invasion and metastasis induced by the m miR-377-3p mimic in the RCC cell lines, which confirmed that miR-377-3p can affect the metastasis of RCC by NOTCH1.

Furthermore, our study confirmed miR-377-3p acts as an intermediary of CircPDK1 and can also regulate NOTCH1 to affect RCC metastasis. In normal condition, miR-377-3p can binding the 3’UTR region of NOTCH1 and inhibit its expression, but when RCC occurs, overexpressed CircPDK1 could function as a sponge by harboring miR-377-3p and induce less available miR-377-3p to binding to the 3’UTR region of NOTCH1 which may lead to the activation of NOTCH1 and promote the tumor metastasis (Fig. 7). Therefore, CircPDK1 can be used as a new biomarker and potential therapeutic target for predicting RCC metastasis. At the same time, in our study, we found that many of the differentially expressed circRNAs in RCC are involved in tumor metastasis and EMT, which makes us think whether the formation of circRNA is closely related to renal cancer and other tumor metastasis processes, and this is worth exploring further.

Conclusions

Our data revealed that CircPDK1 was significantly correlated with tumor metastasis of RCC patients and may function through CircPDK1-miR-377-3p-NOTCH1 axis to promote tumor metastasis process. Therefore, CircPDK1 could be used as a new biomarker for predicting RCC metastasis and a potential target for the tumor therapy.

Abbreviations

circRNAs	Circular RNAs
ncRNAs	Noncoding RNAs
RCC	renal cell carcinoma
ccRCC	clear cell renal carcinoma
ccRCC	microRNA
mRNA	messenger RNA
H&E	Hematoxylin and Eosin
GO	Gene Ontology
KEGG	Kyoto Encyclopedia of Genes and Genomes
sh-NS	sh-Non Specific
MTT	3-(4,5-dimethylthiazol-2-yl)-2,5-diphenyl tetrazolium bromide)
NOTCH1	Notch Homolog 1

Declarations

Authors' contributions

Zhenlin Huang performed the experiments. Jinjian Yang and Yinghui Ding designed the experiments. Lu Zhang performed the mice work. Siyuan He and Hao Li performed the bio information analysis. Xiang Li and Chaohui Gu performed the RNA-seq analysis. Zhankui Jia, Zhibo Jin and Yafei Ding were the major contributor in writing the manuscript. All authors read and approved the final manuscript

Acknowledgements

We sincerely thank the encouragement from the whole member of Dr. Yang Lab.

Competing interests

The authors declare that they have no competing interests.

Availability of data and materials

All data generated or analyzed during this study are included in this published article.

Consent for publication

Not applicable.

Ethics approval and consent to participate

All patients provided informed consent in accordance with the ethical guidelines of the First Affiliated Hospital Zhengzhou University. The study was approved by the Ethics Committee of the First Affiliated Hospital of Zhengzhou University (2019-KY-240).

Funding

The present study was supported by grants from the National Nature Science Foundation of China (Nos. 81570685, 81800614) to J.Y. and L.Z.

References

1. Siegel RL, Miller KD, Jemal A: Cancer statistics, 2018. *CA Cancer J Clin* 2018, 68:7-30.
2. Chen W, Zheng R, Baade PD, Zhang S, Zeng H, Bray F, Jemal A, Yu XQ, He J: Cancer statistics in China, 2015. *CA Cancer J Clin* 2016, 66:115-132.
3. Gupta K, Miller JD, Li JZ, Russell MW, Charbonneau C: Epidemiologic and socioeconomic burden of metastatic renal cell carcinoma (mRCC): a literature review. *Cancer Treat Rev* 2008, 34:193-205.
4. Barata PC, Rini BI: Treatment of renal cell carcinoma: Current status and future directions. *CA Cancer J Clin* 2017, 67:507-524.
5. Capitanio U, Montorsi F: Renal cancer. *Lancet* 2016, 387:894-906.
6. Choueiri TK, Motzer RJ: Systemic Therapy for Metastatic Renal-Cell Carcinoma. *N Engl J Med* 2017, 376:354-366.
7. Meng S, Zhou H, Feng Z, Xu Z, Tang Y, Li P, Wu M: CircRNA: functions and properties of a novel potential biomarker for cancer. *Mol Cancer* 2017, 16:94.
8. Huang XY, Huang ZL, Xu YH, Zheng Q, Chen Z, Song W, Zhou J, Tang ZY, Huang XY: Comprehensive circular RNA profiling reveals the regulatory role of the circRNA-100338/miR-141-3p pathway in

hepatitis B-related hepatocellular carcinoma. *Sci Rep* 2017, 7:5428.

9. Luan W, Shi Y, Zhou Z, Xia Y, Wang J: circRNA_0084043 promote malignant melanoma progression via miR-153-3p/Snail axis. *Biochem Biophys Res Commun* 2018, 502:22-29.
10. Qian DY, Yan GB, Bai B, Chen Y, Zhang SJ, Yao YC, Xia H: Differential circRNA expression profiles during the BMP2-induced osteogenic differentiation of MC3T3-E1 cells. *Biomed Pharmacother* 2017, 90:492-499.
11. Zhao J, Li L, Wang Q, Han H, Zhan Q, Xu M: CircRNA Expression Profile in Early-Stage Lung Adenocarcinoma Patients. *Cell Physiol Biochem* 2017, 44:2138-2146.
12. Zhou B, Yu JW: A novel identified circular RNA, circRNA_010567, promotes myocardial fibrosis via suppressing miR-141 by targeting TGF-beta1. *Biochem Biophys Res Commun* 2017, 487:769-775.
13. Su W, Sun S, Wang F, Shen Y, Yang H: Circular RNA hsa_circ_0055538 regulates the malignant biological behavior of oral squamous cell carcinoma through the p53/Bcl-2/caspase signaling pathway. *J Transl Med* 2019, 17:76.
14. Qu S, Liu Z, Yang X, Zhou J, Yu H, Zhang R, Li H: The emerging functions and roles of circular RNAs in cancer. *Cancer Lett* 2018, 414:301-309.
15. Zhang HD, Jiang LH, Sun DW, Hou JC, Ji ZL: CircRNA: a novel type of biomarker for cancer. *Breast Cancer* 2018, 25:1-7.
16. Di Leva G, Garofalo M, Croce CM: MicroRNAs in cancer. *Annu Rev Pathol* 2014, 9:287-314.
17. Cao Y, Gao X, Yang Y, Ye Z, Wang E, Dong Z: Changing expression profiles of long non-coding RNAs, mRNAs and circular RNAs in ethylene glycol-induced kidney calculi rats. *BMC Genomics* 2018, 19:660.
18. Fang M, Liu S, Zhou Y, Deng Y, Yin Q, Hu L, Ouyang X, Hou Y, Chen C: Circular RNA involved in the protective effect of losartan on ischemia and reperfusion induced acute kidney injury in rat model. *Am J Transl Res* 2019, 11:1129-1144.
19. Wang K, Sun Y, Tao W, Fei X, Chang C: Androgen receptor (AR) promotes clear cell renal cell carcinoma (ccRCC) migration and invasion via altering the circHIAT1/miR-195-5p/29a-3p/29c-3p/CDC42 signals. *Cancer Lett* 2017, 394:1-12.
20. Dabestani S, Marconi L, Bex A: Metastasis therapies for renal cancer. *Curr Opin Urol* 2016, 26:566-572.
21. Mennitto A, Verzoni E, Grassi P, Ratta R, Fuca G, Procopio G: Multimodal treatment of advanced renal cancer in 2017. *Expert Rev Clin Pharmacol* 2017, 10:1395-1402.
22. Liu Y, Gao Y, Li D, He L, Iw L, Hao B, Chen X, Cao Y: LASP1 promotes glioma cell proliferation and migration and is negatively regulated by miR-377-3p. *Biomed Pharmacother* 2018, 108:845-851.
23. Sun C, Li S, Zhang F, Xi Y, Wang L, Bi Y, Li D: Long non-coding RNA NEAT1 promotes non-small cell lung cancer progression through regulation of miR-377-3p-E2F3 pathway. *Oncotarget* 2016, 7:51784-51814.

24. Wang X, Chen T, Zhang Y, Zhang N, Li C, Li Y, Liu Y, Zhang H, Zhao W, Chen B, et al: Long noncoding RNA Linc00339 promotes triple-negative breast cancer progression through miR-377-3p/HOXC6 signaling pathway. *J Cell Physiol* 2019, 234:13303-13317.
25. Zhang J, Li Y, Dong M, Wu D: Long non-coding RNA NEAT1 regulates E2F3 expression by competitively binding to miR-377 in non-small cell lung cancer. *Oncol Lett* 2017, 14:4983-4988.
26. Liu S, Ma X, Ai Q, Huang Q, Shi T, Zhu M, Wang B, Zhang X: NOTCH1 functions as an oncogene by regulating the PTEN/PI3K/AKT pathway in clear cell renal cell carcinoma. *Urol Oncol* 2013, 31:938-948.
27. Sui C, Zhuang C, Sun D, Yang L, Zhang L, Song L: Notch1 regulates the JNK signaling pathway and increases apoptosis in hepatocellular carcinoma. *Oncotarget* 2017, 8:45837-45847.
28. Sun W, Gaykalova DA, Ochs MF, Mambo E, Arnaoutakis D, Liu Y, Loyo M, Agrawal N, Howard J, Li R, et al: Activation of the NOTCH pathway in head and neck cancer. *Cancer Res* 2014, 74:1091-1104.
29. Zhang XS, Hu YH, Gao HY, Lan XW, Xue YW: Downregulation of Notch1 inhibits the invasion and metastasis of human gastric cancer cells SGC7901 and MKN74 in vitro through PTEN activation and dephosphorylation of Akt and FAK. *Mol Med Rep* 2017, 16:2318-2324.
30. Inamura N, Kimura T, Wang L, Yanagi H, Tsuda M, Tanino M, Nishihara H, Fukuda S, Tanaka S: Notch1 regulates invasion and metastasis of head and neck squamous cell carcinoma by inducing EMT through c-Myc. *Auris Nasus Larynx* 2017, 44:447-457.
31. Natsuizaka M, Whelan KA, Kagawa S, Tanaka K, Giroux V, Chandramouleeswaran PM, Long A, Sahu V, Darling DS, Que J, et al: Interplay between Notch1 and Notch3 promotes EMT and tumor initiation in squamous cell carcinoma. *Nat Commun* 2017, 8:1758.

Tables

Due to technical limitations, the tables are only available as a download in the supplemental files section.

Figures

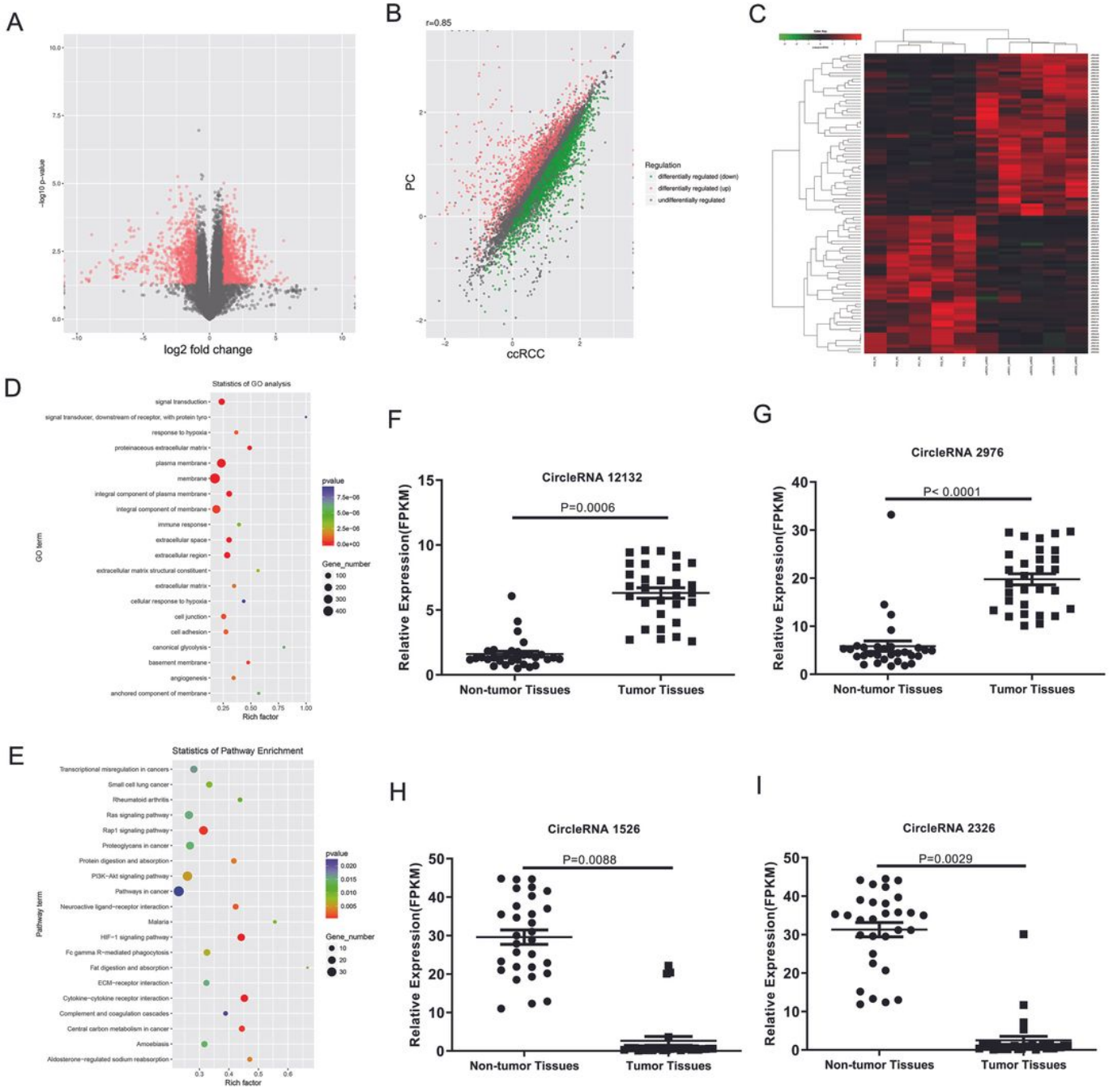

Figure 1

CircRNA expression profile analysis for RCC. A. Five pairs of RCC and paired paratumor tissues (PC) were used to perform circRNA-seq assays to identify the differentially expressed circRNAs in RCC. circRNAs with significant changes are displayed as red dots in the volcano plot. B. circRNA-seq assays analysis results are shown in the scatter plot, in which the upregulated circRNAs are displayed as red dots and the downregulated circRNAs are displayed as green dots. C. The top 100 differentially expressed circRNAs

are displayed in the heat map, and the fold changes are represented by a gradual change in color from red to green. D. GO analysis was performed by analyzing the enrichment OD of differentially expressed protein-coding transcripts (P<0.05). The top 20 enrichment biological processes, cellular components and molecular functions were displayed in the scatter plot, in which the size of the circle represented the number of enriched genes, and the gradual changes in cold to warm color represented the P value. E. KEGG analysis performed by analysis of the enrichment OD differentially expressed protein-coding transcripts (P<0.05), the top 20 enrichment pathways are displayed in the scatter plot, in which the size of the circle represents the number of enriched genes, and the gradual changes in cold to warm colors represents the P value. F-I. RNA was extracted from 30 pairs of RCC and paratumor tissues and reversed into library DNA. qRT-PCR results of 4 circRNAs from 20 randomly selected circRNAs from RNA-seq results are shown in a scatter plot (P<0.05).

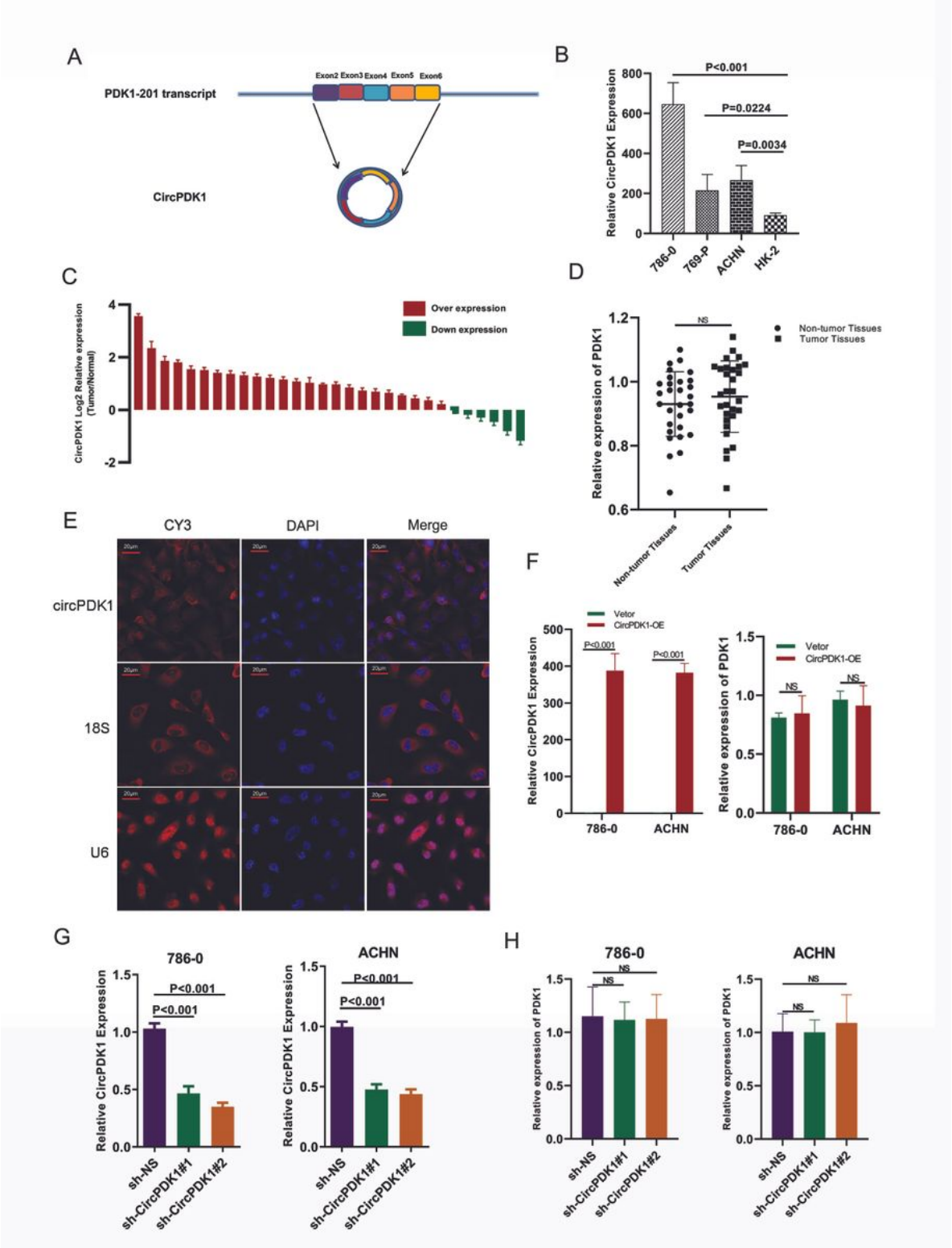

Figure 2

CircPDK1 was upregulated in RCC tissues and associated with tumor metastasis. A. The pattern diagram depicted the relationship between CircPDK1 and PDK1. The line graph represents the PDK1-201 transcript, where boxes of different colors represent different exons. The ring diagram represents the structure of CircPDK1, and the boxes of different colors represent exons corresponding to the PDK1-201 transcript. B. RNA was extracted from 3 types of RCC cell lines and HK-2, which are normal renal cell lines,

and qRT-PCR was used to test CircPDK1 expression in these cell lines. Then, CircPDK1 expression was quantified in other cells by using the HK-2 CircPDK1 expression level as a standard. Data are shown as the means ± SD. The P value was calculated between the indicated groups (N=3). C. qRT-PCR results from 30 pairs RCC and paratumor tissues shown in the column table. The Y-axis value represents the log2 ratio of CircPDK1 expression in RCC tissues compared with that in matched paratumor tissues. The red column represents high CircPDK1 expression in tumor tissues, and the green column represents low CircPDK1 expression in tumor tissues. D. PDK1 expression in our chosed 30 pairs RCC and paratumor tissues detected by using qRT-PCR. Data are shown as the means ± SD. The P value was calculated between the indicated groups (N=3). E. FISH images were taken using a confocal microscope. The red represents the localization of the target gene CircPDK1 or the reference gene U6 and 18S rRNA, and the blue represents DAPI staining for visualizing the nucleus. F. CircPDK1 was overexpressed in 786-0 and ACHN cells, respectively. The expression level of CircPDK1 and PDK1 was verified by qRT-PCR. The blank vector plasmid transfected group was as control groups. G-H. CircPDK1 was knocked down in 786-0 and ACHN cells, respectively. The expression level of CircPDK1 and PDK1 was verified by qRT-PCR. The sh-NS (sh-Non Specific) vector plasmid transfected group was as control groups

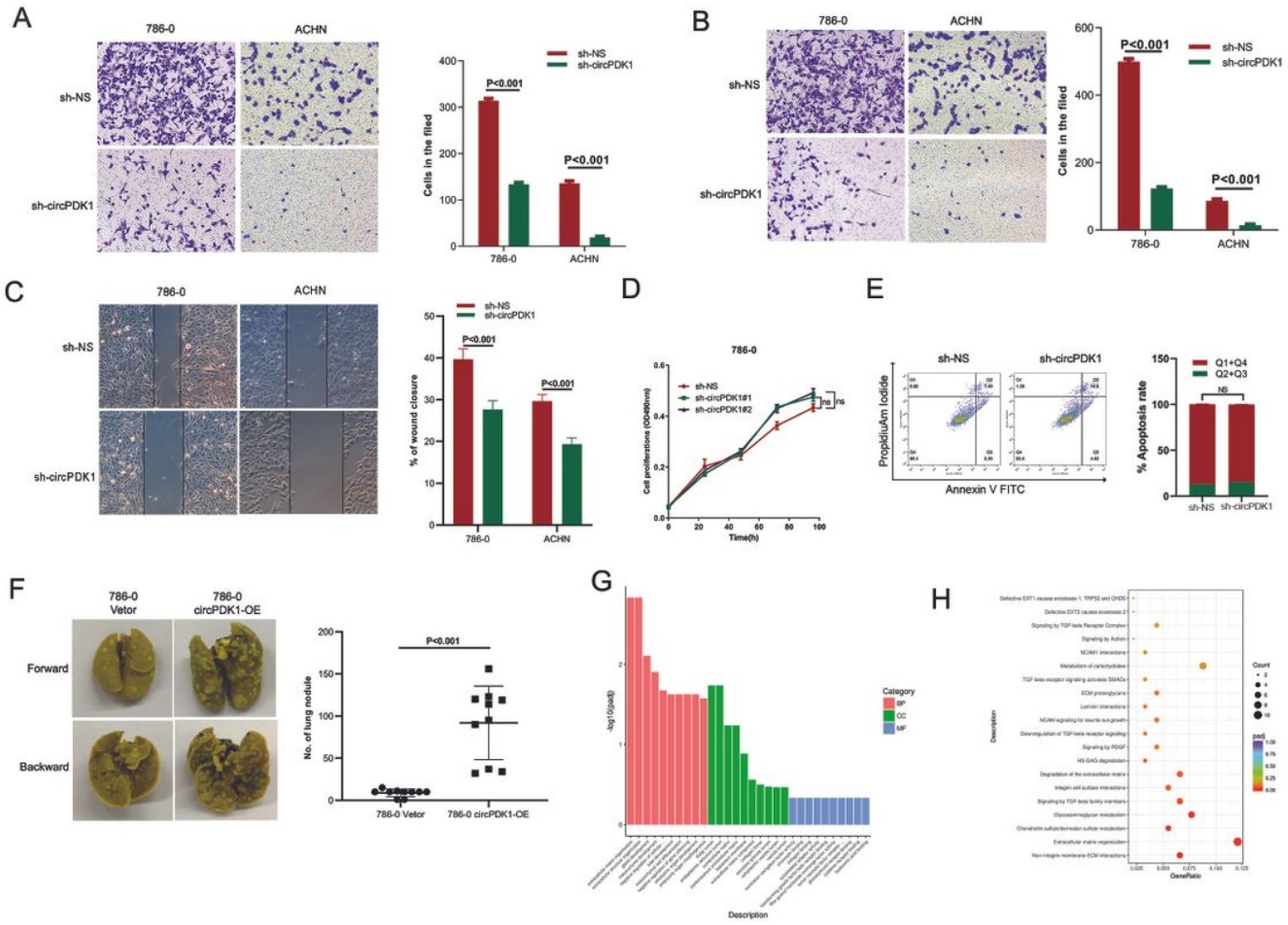

Figure 3

CircPDK1 promotes the invasion and metastasis of RCC cells. A&B. 786-0 and ACHN stable knockdown cells and knockdown control cells were seeded into the transwell plate with or without BD Matrigel in the chamber. And the results were analyzed by Imagine J. C. 786-0 and ACHN stable knockdown cells and knockdown control cells were seeded into 6-well plates and then the tips were used to make a perpendicular scratch on the bottom of the plate. Pictures were taken 12 h later. D. sh-CircPDK1 or sh-NS 786-0 and ACHN stable transfection cell lines were seeded into 96-well plates, cell proliferation was detected by a microplate reader at 0, 24, 48, 72, 96 h at 469 nm. E. 786-0 and ACHN stable knockdown cell lines stained with Annexin V-FITC/ PI for cell apoptosis. Imagines obtained using flow cytometry (Leica, Germany) and analysis with ModFit LT software. F. CircPDK1-OE or the control vector stably transfected 786-0 cells were injected in the tail vein of Six-week-old male BALB/c nude mice and counted the metastatic nodules in the lung tissue one month later, Data are shown as the means ± SD. The P value was calculated between the indicated groups (N=10). G. The potential effects of CircPDK1 on downstream genes and functions were explored by extracting RNA from three different sh-CircPDK1 and sh-NS 786-0 stable knockdown cell lines and reverse transcribed and constructed into library DNA for exon sequencing. The column table shows the top 10 enriched biological processes, cellular components and molecular functions in different colors. H. RNA-seq results from 3 different sh-CircPDK1 and sh-NS 786-0 stable knockdown cell lines were analyzed to determine whether the enrichment of the KEGG pathway may be involved in the function of CircPDK1. The top 20 enrichment pathways are displayed in the scatter plot, in which the size of the circle represents the number of enriched genes, and the gradual changes in cold to warm color represent the P value.

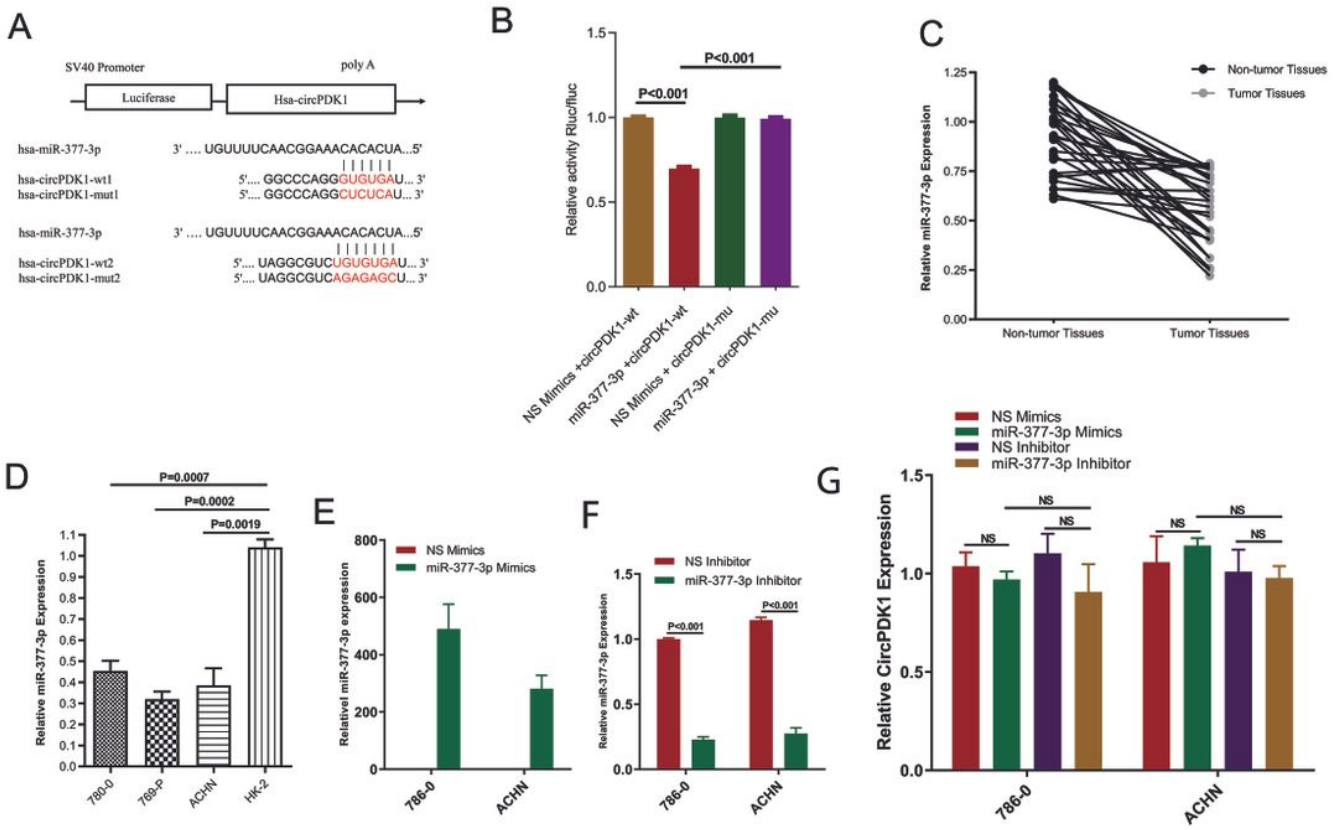

Figure 4

CircPDK1 directly binds to miR-377-3p in RCC. A. Predicted potential binding sites of hsa-miR-377-3p to hsa-circ-PDK1 and hsa-circ-PDK1 mutation site positions. B. has-miR-377-3p plasmid was constructed and cotransfected with wild-type or mutant plasmids containing CircPDK1 into 293T cells, as shown in Fig. 4A. The Renilla luciferase value (Rluc) was recorded as the reporter luminescence value. Normalized Rluc/Fluc values for each well represented the level of mutual binding. Data shown as the means ± SD. The P value was calculated between the indicated groups (N=3). * P <0.05, ** P < 0.01, *** P < 0.001. C. qRT-PCR was used to verify the expression levels of miR-377-3p in 30 pairs of RCC and paratumor tissues and the average expression level in paratumor tissues was used as a standard. D. qRT-PCR was performed to detect the expression of miR-377-3p in RCC cells and HK-2 cells. miR-377-3p was quantified by using the HK-2 miR-377-3p expression level as a standard. Data are shown as the means ± SD. The P value was calculated between the indicated groups (N=3). E-G. 786-0 and ACHN cells were transfected with miR-377-3p mimics and inhibitors or their negative control, respectively, and then the expression level of miR-377-3p and CircPDK1 was verified in each group. NS indicated no significant change. Data are shown as the means ± SD. The P value was calculated between the indicated groups (N=3).

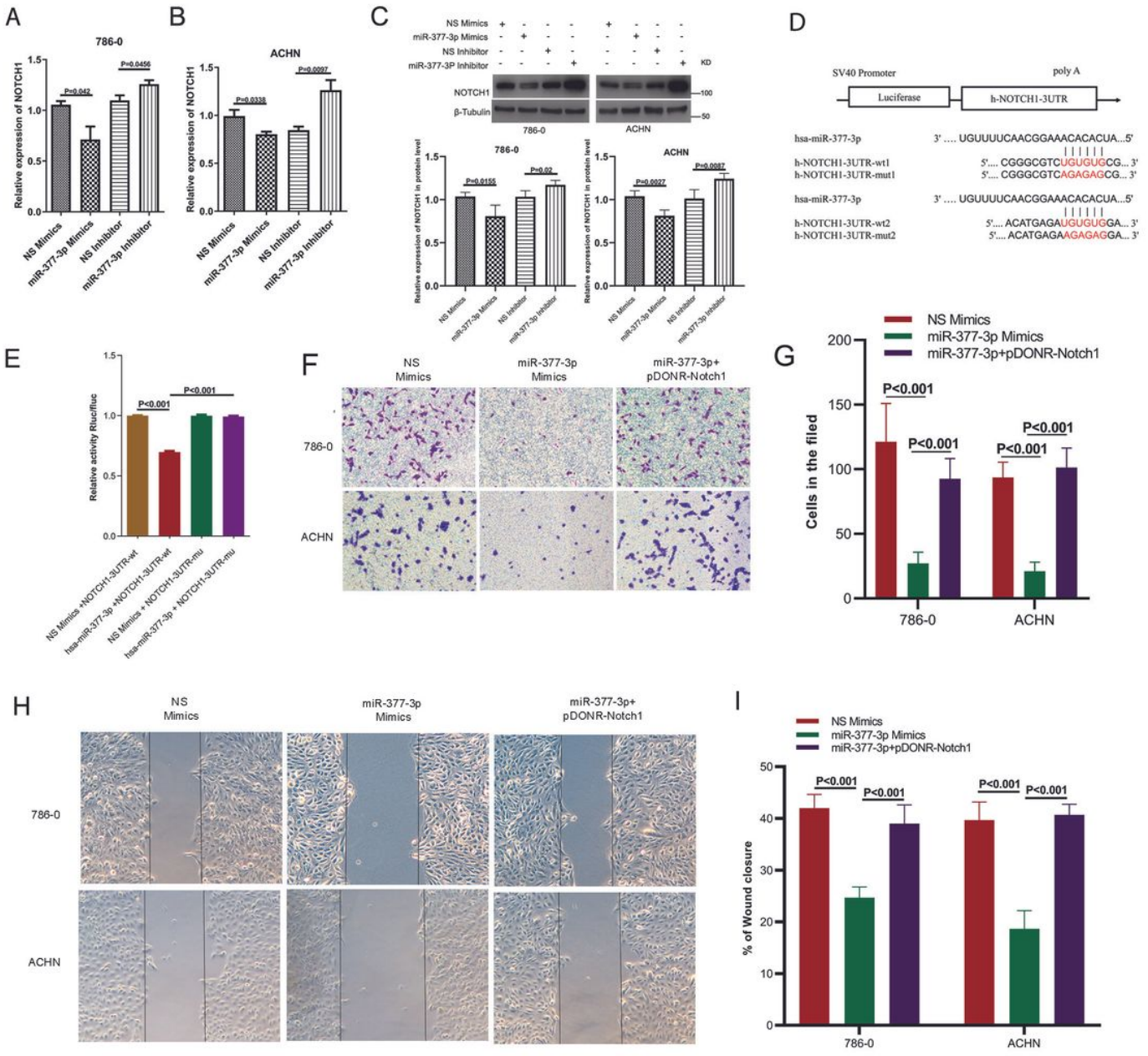

Figure 5

MiR-377-3p suppresses RCC cell invasion and metastasis by targeting NOTCH1. A&B. 786-0 and ACHN cells were transfected with miR-377-3p mimics and inhibitors or their negative controls, respectively, and the expression level of NOTCH1 was verified in each group. Data are shown as the means ± SD. The P value was calculated between the indicated groups (N=3). C. 786-0 and ACHN cells were transfected with miR-377-3p mimics and inhibitors or their negative control, respectively, and Western blotting was used to verify the expression level of each group. β-tubulin was used as a control. D. Predicted potential binding sites of hsa-miR-377-3p to hsa-NOTCH1 and hsa-NOTCH1 mutation site positions. E. has-miR-377-3p plasmid was constructed and cotransfected with wild-type or mutant NOTCH1 plasmid into 293T cells as shown in Fig. 5D. The cells were treated using the method in Fig. 4F to verify the normalized Rluc/Fluc

values for each well representing the level of mutual binding. The P value was calculated between the indicated groups (N=3). F&G. 786-0 and ACHN cells were transfected with miR-377-3p negative control (NS mimics), miR-377-3p or miR-377-3p with pDONR-Notch. The cells were treated using the method in Fig. 3B to verify the migration ability of each group. Data shown as the means ± SD. The P value was calculated between the indicated groups (N=3). H&I. 786-0 and ACHN cells were transfected with the miR-377-3p negative control (NS mimics), miR-377-3p or miR-377-3p with pDONR-Notch, and the cells were treated by using the method in Fig. 3C to verify the invasion ability of each group. Data are shown as the means ± SD. The P value was calculated between the indicated groups (N=3).

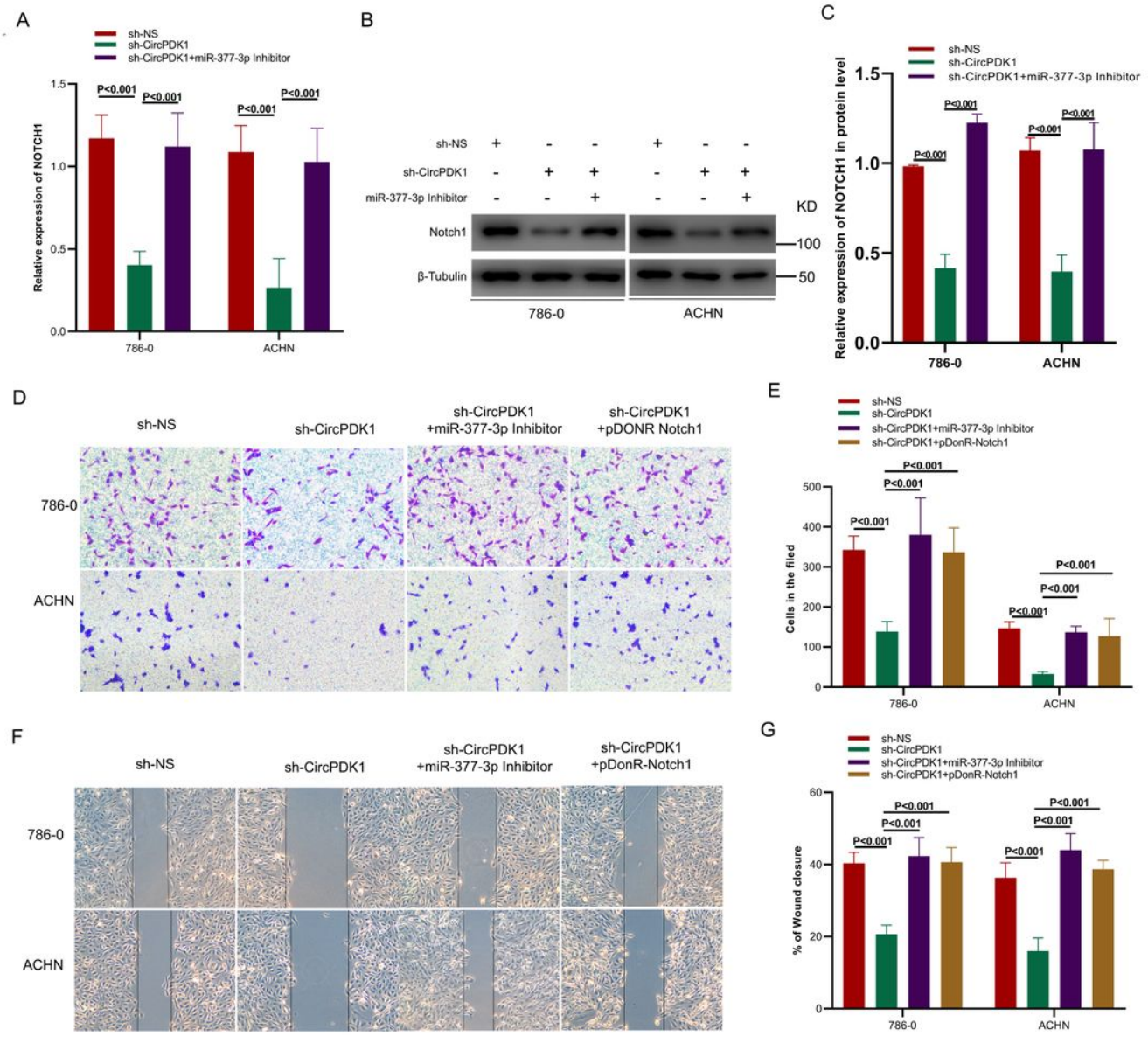

Figure 6

CircPDK1 promotes RCC cell invasion and metastasis by sponging miR-377-3p and upregulating NOTCH1. A. sh-NS or sh-CircPDK1 was transfected with or without miR-377-3p inhibitors into 786-0 and ACHN stable cell lines, and the cells were seeded into 6-well plates; qRT-PCR was used to verify the expression level of NOTCH1 in each group. The P value was calculated between the indicated groups (N=3). B. sh-NS or sh-CircPDK1 was transfected with or without miR-377-3p inhibitors into 786-0 and ACHN stable cell lines, and the cells were seeded into 6-well plates; Western blotting was used to verify the expression level of NOTCH1 in each group. β-tubulin was used as a control. C&D. sh-NS or sh-CircPDK1 was transfected with or without miR-377-3p inhibitors and pDONR-NOTCH1 into 786-0 and ACHN stable cell lines, and the cells were seeded into 6-well plates and treated by using the method in Fig. 3D&E to verify the migration ability of each group. Data are shown as the means ± SD. The P value was calculated between the indicated groups (N=3). E&F. sh-NS or sh-CircPDK1 was transfected with or without miR-377-3p inhibitors and pDONR-NOTCH1 into 786-0 and ACHN stable cell lines to verify the invasion ability of each group. The cells were treated using the method in Fig. 3B to verify the migration ability of each group. Data shown as the means ± SD. The P value was calculated between the indicated groups (N=3). G. sh-NS or sh-CircPDK1 was transfected with or without miR-377-3p inhibitors and pDONR-NOTCH1 into 786-0 and ACHN stable cell lines, cells were treated by using the method in Fig. 3C to verify the invasion ability of each group. Data are shown as the means ± SD. The P value was calculated between the indicated groups (N=3).

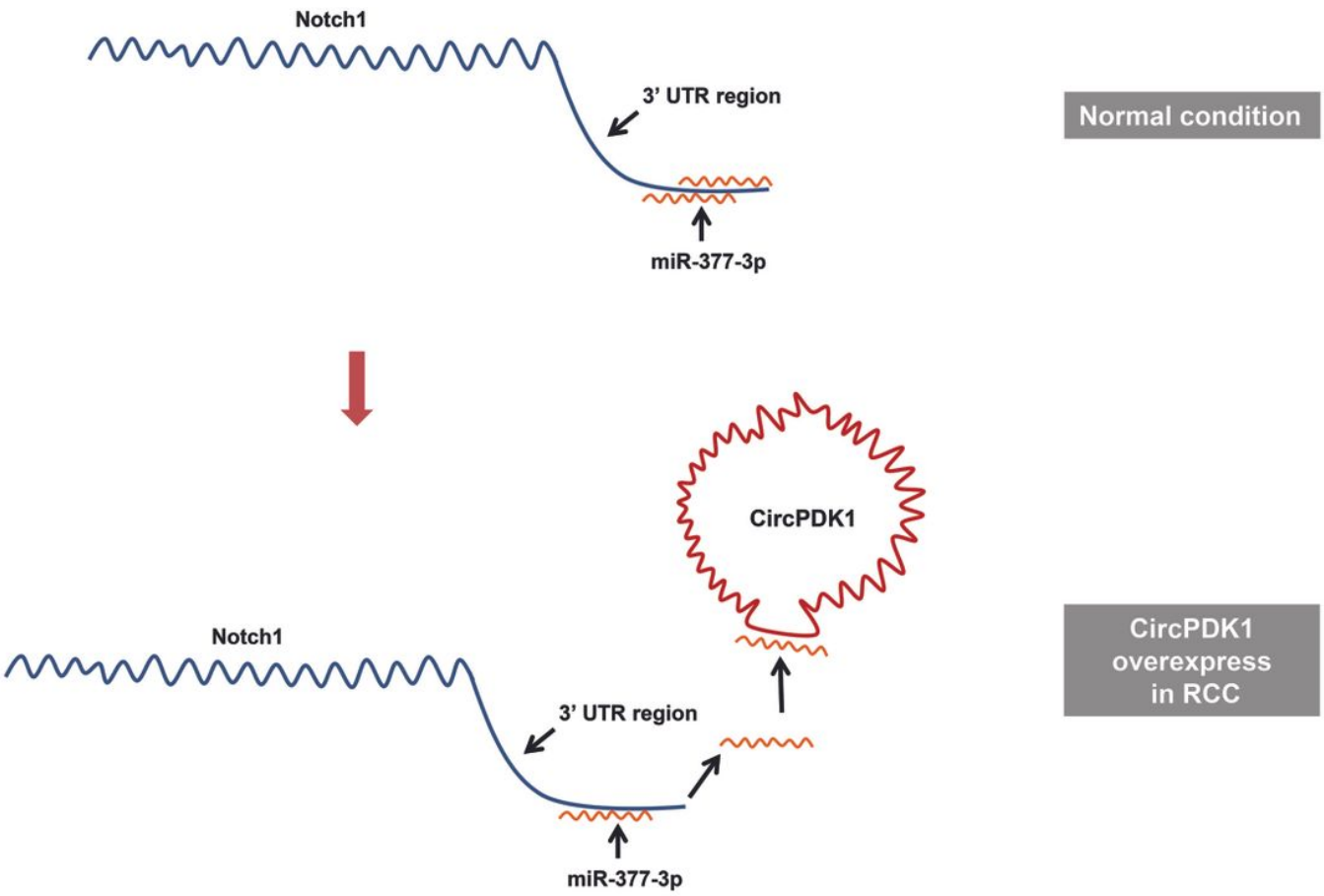

Figure 7

Working model. In normal condition, miR-377-3p binds on the 3'UTR region of NOTCH1 mRNA and inhibits its function. While in the RCC, circPDK1 is overexpressed and adsorbs miR-377-3p by the sponge effect, which decreases the binding of miR-377-3p on the 3'UTR region of NOTCH1 mRNA and promotes NOTCH1 function in return.

Supplementary Files

This is a list of supplementary files associated with this preprint. Click to download.

- Table2.xlsx
- Table3.xlsx
- Table1.xlsx
- Supplemental1.docx